IRS-aided Network Scheme Supports Unmanned Aerial Vehicle Communication

Pham The Hien, Van Phu Tuan, and Ic-Pyo Hong

***Abstract*—Intelligent reflecting surface (IRS) and unmanned aerial vehicle (UAV) are forecasted to be extensively used in the forthcoming wireless system. In order to enhance the operational efficiency of UAVs in the urban areas, this paper proposes employing IRS equipped on the rooftop of buildings to create ground-to-air data links between the terrestrial base stations (BSs) and UAVs without any change in the terrestrial infrastructure. An optimization problem aiming to maximize the cumulative achievable data rate (CADR) and minimize the UAV's operational duration via altering the configuration of the IRS network, i.e., the phase profiles and reflecting angles, and the UAV's trajectory has been investigated. To deal with this optimization problem, firstly, we analyze the far-filed radiation pattern of all IRSs to construct the received signal strength (RSS) map over the considered region for a given setup of the activated BS and IRS networks. Then, this map is used to construct the designated BS-IRS-UAV paths (DBIUPs) that are the best paths between neighboring BSs obtained through optimizing the IRS network. Secondly, we develop heuristic algorithms (HAs) to select appropriate DBIUPs to build the optimize UAV's trajectory for any departing and landing positions. The simulation results show that the proposed scheme significantly improves the CADR and reduces the disconnected distance/duration (DD) of considered UAV communication, and the proposed algorithm has a good convergence.**

***Index Terms*—Heuristic algorithm-based optimization, intelligent reflecting surface, phase shift optimization, trajectory optimization, and UAV communication.**

I. Introduction

UNMANNED aerial vehicles have commenced a huge range of applications in several fields, both in the military and civilian. The ability to equip various types of sensors to a flying device makes it become a wealthy source of information which can be used for missions such as surveillance, rescue management, cargo delivery, observation, tracking from the air, etc. [1], [2]. Therefore, the requirement of achieving high-speed and stable air-to-ground wireless links is anticipated to play an important role in future UAV communication systems [3] and the UAV control and path planning also become the crucial problems [4], [5]. Moreover, there are so many challenges which the UAV communication have to be encountered, especially in urban areas where the blockages caused by common objects such as the buildings and trees are the prominent challenges [6] which can lead to the issues of poor coverage and connectivity.

To address these issues, IRS, a large surface made from metallic and dielectric materials, and a large number of configurable electronic elements, has recently emerged as a potential solution due to its capacity of controlling the property of wireless signals [7], [8]. The effectiveness of using IRS in enhancing the performance of both terrestrial and airborne wireless communication has been validated in many recent publications [9]–[14]. Specifically, with the ability of intelligently tuning the amplitude and phase shifts of passive elements, IRS are able to adjust the wireless channel and generate a beneficial wireless propagation environment [9]–[11], and thus has been proposed to improve the performance of wireless communications and bypass obstacles [12]–[14]. For IRS-enabled air-to-ground wireless communication, there are two main approaches which depend on the IRS installation. The first approach uses static IRSs attaching to the buildings to reflect the wireless signal toward the UAVs. In [15], in order to maximize average achievable rate of the system, the authors studied a static IRS-aided UAV system and proposed an optimization algorithm to optimize the UAV's trajectory and the passive beamforming factors. Whilst, the study in [16] proposed a secure IRS-assisted UAV system in which the static IRS is utilized to assist the secure downlink communication between a UAV-mounted transmitter and a legitimate receiver in the presence of an eavesdropper. By optimizing the UAV's trajectory, transmit power, and IRS's phase shift, the secrecy rate of this proposed system is maximized. Additionally, the author in [17] proposed algorithms to minimize the bit error rate by jointly optimizing the UAV trajectory, IRS phase shift matrix, and IRS scheduling while minimizing the data rate requirement for the UAV. Another approach investigates mobile IRS where the IRS is mounted on UAV and provides better wireless links to terrestrial users. Inheriting the high mobility property of the UAV, the UAV-mounted IRS can be easily placed at any location and altitude with a low cost for deployment. The works [18] show that the UAV-mounted IRS can give a notable improvement in data rate for a non-orthogonal multiple access (NOMA) multiple-input- single-output (MISO) system. Besides the position optimization, the transmit beamforming vector and the IRS's phase shift matrix were jointly optimized to archive the optimum system performance. The study of the energy efficiency (EE) of a

Manuscript received March 26, 2022 revised July 10, 2022; approved for publication by Zhengyu Zhu, Guest Editor, August 16, 2022.

This work was supported in part by the Basic Science Research Program under Grant 2020R1I1A3057142, in part by the Priority Research Center Program through the National Research Foundation under Grant 2019R1A6A1A03032988, and in part by the Underground City of the Future Program funded by the Ministry of Science and ICT.

P. T. Hien and I.-P. Hong are with the Department of Information and Communication Engineering, Kongju National University, Cheonan 314701, South Korea, email: phamhien.tn9190@outlook.com and iphong@kongju.ac.kr.

V. P. Tuan is with the Faculty of Electrical and Electronics Engineering, Dong A University, Da Nang city, Vietnam, email: tuanvp@donga.edu.vn.

I.-P. Hong is the corresponding author.

Digital Object Identifier: 10.23919/JCN.2022.000036

1229-2370/22/$10.00 © 2022 KICS

cooperative communication system was investigated in [19] where a UAV-mounted IRS served as a relay to forward the signal broadcasted by a multiple-antenna base station to single-antenna cell-edge users. A joint optimization algorithm of the power allocation and the IRS phase shift matrix was designed for the goal of maximizing the overall EE.

Most of the existing works employed IRS as a single reflector to improve the downlink wireless communication system wherein the IRS was being in charge of a mobile BS or a relay, and did not investigate the effect of radiation pattern on channel property. In this paper, we investigate the practical model for the radiation pattern of IRS and its effect on UAV uplink communication. Our proposed system consists of a network of terrestrial BSs that are purposely deployed for terrestrial communication and a network of IRSs placed on the top of the building surrounding the those terrestrial BSs. The reflected signals from the IRSs allow the UAV to communicate with the terrestrial BSs. The UAV departs and lands at determined positions. During the UAV's travel, there is a demand for communicating with the terrestrial BS network for some specific tasks. Our goal is to maximize the CADR between UAV and the terrestrial BS network and minimizing the traveling distance while carrying out its tasks. The main contributions of this paper are summarized as follows.

- In order to accomplish this target, firstly, the far-field radiation pattern of the reflection on an IRS is characterized using the physic optic technique [11]. This result allows us to evaluate the RSS at a custom position. Extending our investigation to the networks of BSs and IRS and combining all the RSS, we can build a DBIUP map for the UAV's operational area that stored the best RSS at specific directions and the respective configuration for the BS and IRS networks, i.e. the activation schedule for the BSs, the selected IRSs, and the reflection setup of these selected IRSs, to archive this best RSS.
- Next, the two HAs, namely genetic algorithm (GA) and particle swarm optimization (PSO), are designed to find the UAV's optimal trajectory to archive the goals, i.e., maximizing the CADR and minimizing the UAV's operational duration, using the obtained DBIUP map. Using the DBIUP map and UAV's optimal trajectory, the optimal configuration for the BS and IRS networks are revealed.
- Finally, we prepare the numerical results for the optimal CADR and optimal trajectory for performance evaluation. The numerical results show that the DBIUP map plays an important role in optmizing the operation of the UAV, the BS and IRS networks. The proposed algorithms effectively provides great CADR to the UAV. The GA outperforms the PSO algorithm in finding the optimal BS-IRS-UAV path (BIUP). For instance, the GA brings the higher performance with less convergence duration. In addition, the results also reveal the effects of various key parameters, such as the IRS's size, the number of IRS panels around the BSs and the transmit power, on the UAV communication schemes which provide the informative views of the system design.

The rest of the paper is organized as follows. In Section II, the system model and preliminary results for RSS model are presented. The HA-based BIUP algorithms are investigated in Section III. Section IV illustrates and discusses the numerical results followed by the Section V as the conclusion.

II. System Model and Preliminary Results for RSS Model

In this section, firstly, we briefly describe the design of the proposed IRS scheme, examine the scattered field from a single IRS, and develop the RSS model for the signal sent from a source and reflected from that IRS. Then, we extend our study for the RSS model to the scenario consisting of multiple BSs and IRSs. After that, the optimal RSS model and the respective configuration for the IRS network are analyzed. Finally, the DBIUP map, which allows good designs for the UAV's trajectory, is developed based on the optimal RSS map.

A. System Model and RSS Model Construction

We consider the system model illustrated in Fig. 1. We assume that there are some IRSs deployed on top of the building surrounding a terrestrial BS (Fig. 1(a)), these IRS aims to support the communication between a UAV and a BS by reflecting the signals sent by BS to the UAV. It is important to note that the type of IRS we employ in this study is the adaptive IRS whose phase profile does not change over time, compared to the dynamic IRS which adjusts the phase profile based on the carrier frequency (usually from a few GHz to a few tens of GHz) when the reflected signal is out of the plane that contains the BS and the normal vector of the IRS. There are only two situations that make the adaptive IRS change the phase profile:

- When the target UAV is moving, the IRS automatically steers the wave beam to the UAV.
- When BS is moved to another position, the IRS automatically adjusts the reflection direction to make sure that the reflected signal is in the same direction as the plane that contains the BS and the normal vector of the IRS

To construct the RSS model, we need to study the behavior of the reflected electromagnetic (EM) wave and the EM propagation. Due to the long distance between the BS and IRS (as shown in Figs. 1(a) and 1(b)), when the BS broadcasts signals, the incident wave at the IRS can be considered as a plane wave which is formulated as [11], [20]:

$$\mathbf{E}_{\text{inc}}(\theta_{\text{inc}}) = \mathbf{e}_x E_{\text{inc}} e^{-j\boldsymbol{\beta}_{\text{inc}}(\theta_{\text{inc}})\cdot\mathbf{r}}, \tag{1}$$

$$\mathbf{H}_{\text{inc}}(\theta_{\text{inc}}) = \mathbf{e}_{\text{inc}}(\theta_{\text{inc}})\frac{E_{\text{inc}}}{\eta} e^{-j\boldsymbol{\beta}_{\text{inc}}(\theta_{\text{inc}})\cdot\mathbf{r}}, \tag{2}$$

where θ_{inc} is the angle of incident EM field, E_{inc} is the magnitude of the incident E-field, $\boldsymbol{\beta}_{\text{inc}}(\theta_{\text{inc}}) = \beta(\sin(\theta_{\text{inc}})\mathbf{e}_y - \cos(\theta_{\text{inc}})\mathbf{e}_z)$ is the phase constant vector which also indicates the propagation direction of the wave plane, $\beta = 2\pi/\lambda_0$ is the phase constant, λ_0 is the wavelength, $\mathbf{r}$ is the position vector in rectangular coordinates, $\mathbf{e}_{\text{inc}}(\theta_{\text{inc}}) = -\cos(\theta_{\text{inc}})\mathbf{e}_y - \sin(\theta_{\text{inc}})\mathbf{e}_z$ is the direction of the H-field, and η is the characteristic impedance of the medium.

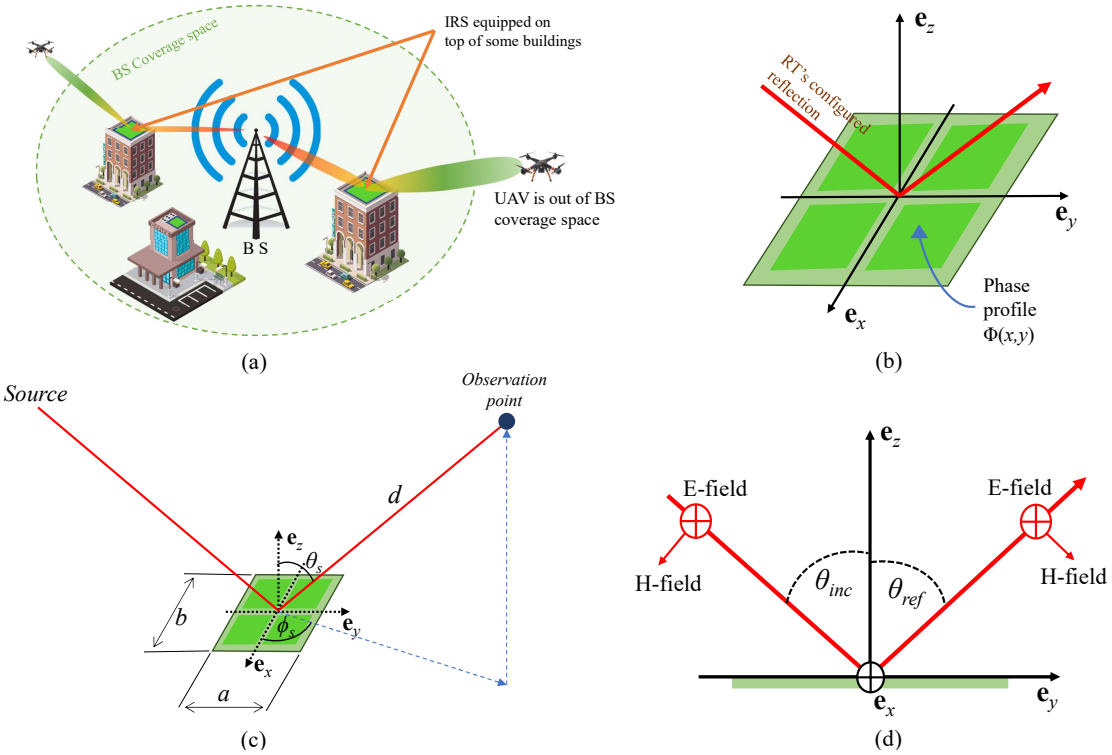

Fig. 1. (a) The system model consisting one BS and multi IRSs (b) The reflection on the RT (c) RSS model of a single IRS and (d) the side view of the reflection.

When the IRS is configured to reflect the EM field at a desired angle θ_{ref}, its phase profile $\Phi(x, y)$ must obey the following rule [11, eq. (13)]:

$$\Phi(x, y) = \beta \left(\sin(\theta_{\text{inc}})y - \sin(\theta_{\text{ref}})y\right). \tag{3}$$

Proposition 1. *Assume that the IRS with a size of $a \times b$ is purposely configured for a reflection* $\text{REF}\left[(\theta_{inc}, \phi_{inc} = 90°) \rightarrow (\theta_{ref}, \phi_{ref} = 90°)\right]$[1] *(we use* $\text{REF}(\theta_1, \theta_2, \varphi)$ *to denote the reflection on the IRS of a wave field hitting the IRS at an angle θ_1 and departing at angle θ_2 with the phase shift φ), and the incident EM field at the IRS is* $(\boldsymbol{E}_{inc}(\theta_{inc}, \phi_{inc} = 90°), \boldsymbol{E}_{inc}(\theta_{inc}, \phi_{inc} = 90°))$ *(same as the configuration illustrated in Figs. 1b-1c). The squared magnitude of the scattered field at an observing position (d, θ_s, ϕ_s) (we consider the reflecting EM field as a EM scattering process) is calculated as*

$$\begin{aligned} S\left(\theta_s, \phi_s; E_{\text{inc}}^2, d\right) = \frac{E_{\text{inc}}^2}{d^2}\left(\frac{ab}{\lambda_0}\right)^2 \cos\left(\theta_{\text{inc}}\right)\cos\left(\theta_{\text{ref}}\right) \\ \times \left(\cos^2(\theta_s)\cos^2(\phi_s) + \sin^2(\phi_s)\right) \\ \times \operatorname{sinc}^2\left(\tfrac{1}{2}a\beta\sin(\theta_s)\cos(\phi_s)\right) \\ \times \operatorname{sinc}^2\left(\tfrac{1}{2}b\beta\left(\sin\left(\theta_s\right) - \sin\left(\theta_{\text{ref}}\right)\right)\right), \end{aligned} \tag{4}$$

[1]Note that if $\phi_{\text{inc}} \neq \phi_{\text{ref}}$, the IRS must reconfigure its phase profile at the frequency of the incident EM wave to guarantee the desired reflection. This causes the high cost and power consumption. Hence, without loss of generality, we set $\phi_{\text{inc}} = \phi_{\text{ref}} = 90°$. At this scenario, the IRS does not need to reconfigure its phase profile.

where d, θ_s and ϕ_s are respectively the distance, $sinc(x) = sin(x)/x$, zenith angle and azimuth angle from the center of the IRS to the observer's position as illustrated in Fig. 1(c).

Proof. see Appendix A. □

Proposition 2. *Using the squared magnitude given in Proposition 1, the path loss model for the signal, that is sent by a transmit (Tx) antenna and reaches a receive (Rx) antenna via a IRS, is measured by:*

$$\alpha_{\text{RT}} = \sqrt{\frac{1}{2\eta}\left(\frac{\lambda^2 G_{\text{Rx}}(\theta_{\text{Rx}\rightarrow\text{IRS}})}{4\pi}\right) S\left(\theta_{\text{IRS}\rightarrow\text{Rx}}; E_{\text{inc}}^2, d_{\text{IRS}\rightarrow\text{Rx}}\right)}, \tag{5}$$

where $E_{\text{inc}}^2 = 2\eta P_0 G_{\text{Tx}}(\theta_{\text{Rx}\rightarrow\text{IRS}})/4\pi d_{\text{Tx}\rightarrow\text{IRS}}^2$ is the squared magnitude of the incident E-field, P_0 is the transmit power, $G_{\text{Tx}}(\cdot)$ and $G_{\text{Rx}}(\cdot)$ are respectively the directivity models of the Tx and Rx antennas, $\theta_{\text{Tx}\rightarrow\text{IRS}}$ and $\theta_{\text{Rx}\rightarrow\text{IRS}}$ are respectively the Tx and Rx angles of the links from the Tx and Rx antennas to the IRS, and $d_{\text{Tx}\rightarrow\text{IRS}}$ and $d_{\text{Rx}\rightarrow\text{IRS}}$ are respectively the distances of the $\text{Tx} \rightarrow \text{IRS}$ *and* $\text{Rx} \rightarrow \text{IRS}$ *links.*

B. Preliminary results of the DBIUP map

Using the theoretical results in Section II-A, we can extend our study to the case of scattering field from the BS and IRS network. The goal of this sections to construct a RSS map and the DBIUP map. In this study, we consider a BS and IRS network in a 16 km square area as four km of X range and Y range. There are 19 terrestrial BSs situated in hexagonal

TABLE I
SYSTEM PARAMETERS FOR SIMULATION.

$\{f_0, \lambda_0\}$	2.4 GHz, 0.125 m
P_0	$\{10, 20, 30, 40,$ and $50\}$ W
N_0	-60 dBm
Number of BS	19
Number of IRS (number of IRSs per BS)	76(4), 95(5), 114(6)
IRS sizes: $a \times b$	$\{5\lambda_0 \times 5\lambda_0, 10\lambda_0 \times 10\lambda_0$ $20\lambda_0 \times 20\lambda_0, 25\lambda_0 \times 25\lambda_0\}$
IRS size	$2 \times N_c$ RTs (assume that IRS is assembled by many reflecting tiles (RTs) each has a size $a \times b$)
BS height	60–70 m
IRS height	30–40 m
Radius of the map	2500 m
Radius of each cell	500 m
Distance between BS and IRS	$\sim$ 100 m

distribution. In this study, we conduct various IRS schemes with the number of IRS surrounding each BS is from four to six separated by an angle of 60 degrees and the distance from each IRS to its BS is around 100 m. The Tx power of BSs varies from 10 to 50 W. Unless otherwise specified, the coordinate distribution (in meters) of BSs and IRSs in our scheme is illustrated in Figs. 2(a) and 2(b), and the system parameters are listed as in Table I.

The Figs. 2(c) and 2(d) demonstrate the DBIUP map of the area under consideration derived by applying the mathematical approach in Section II-A. In this DBIUP map, there are six IRSs per each BS as well as the source transmit power P_0 is 30 W. It can be clearly seen that, the further the observation point situated from the IRS, the lower achievable RSS at that point. Furthermore, the strongest received signals are located on the link where the angle of ϕ_s in (4) is equal 90°. Since the reflection coefficients of the static IRS do not change during the communication, the static IRS can only perform the reflection $\mathrm{REF}\left((\theta_{\text{inc}}, \phi_{\text{inc}} = 90^\circ) \rightarrow (\theta_{\text{inc}}, \phi_{\text{inc}} = 90^\circ)\right)$.

III. HEURISTIC ALGORITHM-BASED BIUP NETWORK OPTIMIZATION.

In Section II-B, we have successfully constructed the DBIUP map, however, the information from this map is not enough to design the trajectory for the UAV, such as, how the UAV moves from one DBIUP to another DBIUP to gain a shorter traveling distance, lower disconnected time, and higher CADR. To solve this problem, we firstly find the transit point (TP) on the DBIUP of one BS and another TP on the DBIUP of one of its neighbors (NB). These TPs are employed to establish the communication link for UAVs between two BSs. Two HA algorithms, namely GA and PSO, are utilized and described in the later subsections. The goal of these two HAs is to find the optimum TPs between two nearby DBIUPs. This procedure is repeated for all of the remaining NBs of the considered BS so that all communication links of that BS with its NBs can be determined. The same process is applied to all of the remaining BSs to construct the optimal BIUP network over the map. Based on these results, the UAV can determine the optimum trajectory to move from a departure position to a landing position.

TABLE II
HA-BASED BIUP NETWORK OPTIMIZATION ALGORITHM.

Input: The list identification number (IDs) of K BSs (I_{BS}), the number of NB per each BS (L), list IDs of L NBs of each BS (I_{NB}), the DBIUP information of all BSs including: the data rate at all points on the DBIUP (R) and their coordination (x, y), GA flag (ga_flag = 0 or 1).
Output: Data rate at the TP on DBIUP of BS ($R_{\text{TP\_BS}}$), data rate at the TP on the DBIUP of NB ($R_{\text{TP\_NB}}$), the distance between those two TPs (d_{TP}).

```
K = length of I_BS;
for k = 1 to K do                          % Loop over all BSs
  for l = 1 to L do                        % Loop over all NBs of the kth BS
    R_BS = R(I_BS(k));                     % Get the data rate at all M points
                                           % on the DBIUP of the kth BS
                                           % to the lth NB.
    R_NB = R(I_NB(l));                     % Get the data rate at all N points
                                           % on the DBIUP of the lth NB to
                                           % the kth BS.
    (x_BS, y_BS) = (x(I_BS(k)), y(I_BS(k)));
                                           % Get the coordination of
                                           % all M points on the DBIUP
                                           % of the kth BS.
    (x_NB, y_NB) = (x(I_NB(l)), y(I_NB(l)));
                                           % Get the coordination of
                                           % all N points on the DBIUP
                                           % of the lth NB.
    if ga_flag == 1 then
      (R_TP_BS(k)(l), R_TP_NB(k)(l), d_TP(k)(l))
      = GA_based(R_BS, R_NB, (x_BS, y_BS), (x_NB, y_NB));
                                           % Use genetic algorithm (GA) to
                                           % solve problem.
    else
      (R_TP_BS(k)(l), R_TP_NB(k)(l), d_TP(k)(l))
      = PSO_based(R_BS, R_NB, (x_BS, y_BS), (x_NB, y_NB));
                                           % Use particle swarm optimization
                                           % (PSO) to solve problem.
    end if
  end for
end for
return (R_TP_BS, R_TP_NB, d_TP)
```

More specifically, let's denote M as the total number of all possible TPs on the DBIUP of one BS, and N is the total possible TPs on the DBIUP of one of its NB. The distance between two adjacent TPs on every DBIUP is 2 m. (Note that the values of M and N can be different for each pair of a BS and its NB). The proposed algorithm is expressed as in Table II.

A. GA-based BIUP Optimization

In our GA, each chromosome consists three parameters, the first one is the data rate at a mth TP on the DBIUP of the BS denoted as R_m^{BS}, the second one is the data rate at a nth TP on DBIUP of its NB as R_m^{NB}. These data rates can be deduced from the RSS information at those TPs. And the last parameter of a chromosome is the distance between BS and its NB through two of those TPs as shown in Fig. 3. Therefore, the structure of the chromosomes is defined as $Chr = [R_m^{\text{BS}}, R_n^{\text{NB}}, d_{mn}]$. The fitness function needs to ensure that the BIUP provide good CADR for the

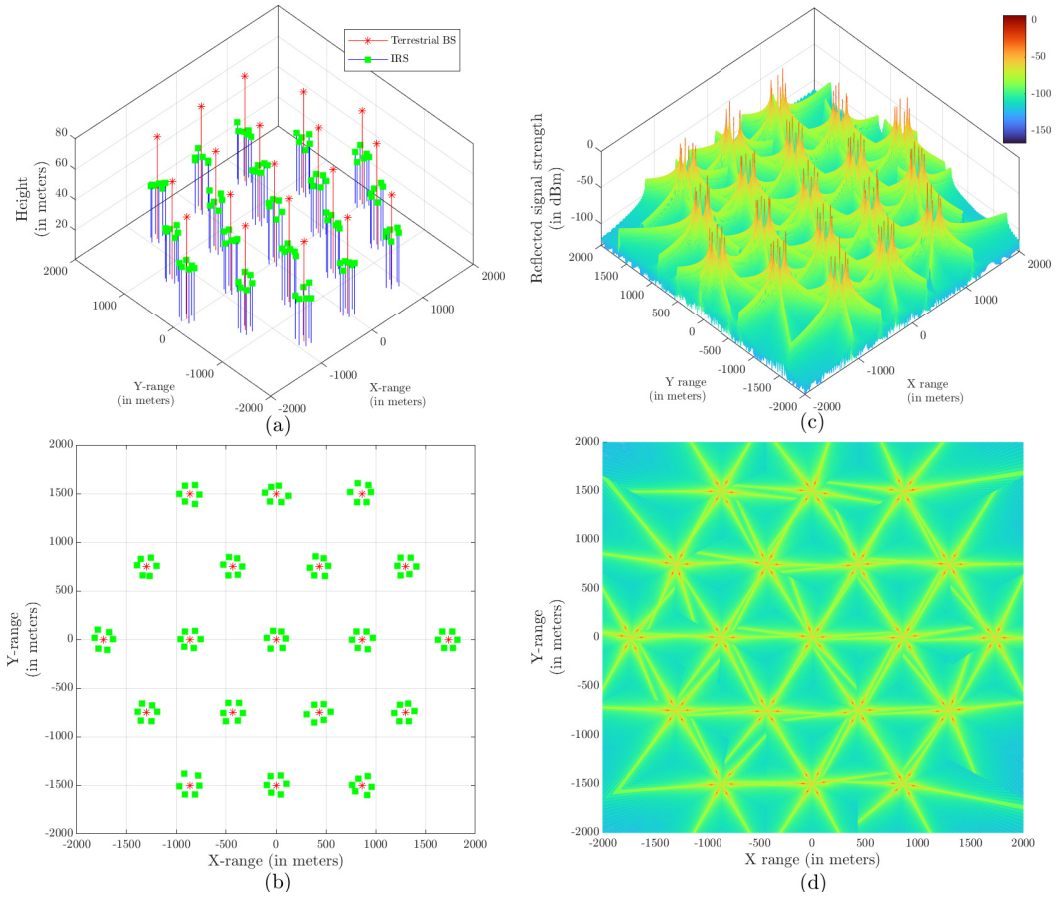

Fig. 2. The BS and IRS distributions: (a) 3D view, and (b) 2D view. And the constructed DBIUP map: (c) 3D view and (d) 2D view.

UAV while the distance between two BS must be minimized with acceptable disconnection duration (if it happens). The chromosomes which yield higher fitness values are the better BIUPs. With these criteria, the fitness function is designed as follows.

$$f(\text{Chr}) = \left(\begin{array}{l} R_m^{\text{BS}} + R_n^{\text{NB}} \\ + \left(\begin{array}{l} \|(x_{\text{BS}}, y_{\text{BS}}) - (x_m^{\text{BS}}, y_m^{\text{BS}})\|_2 \\ + \|(x_m^{\text{BS}}, y_m^{\text{BS}}) - (x_n^{\text{NB}}, y_n^{\text{NB}})\|_2 \\ + \|(x_{\text{NB}}, y_{\text{NB}}) - (x_n^{\text{NB}}, y_n^{\text{NB}})\|_2 \end{array} \right)^{-1} \end{array} \right), \quad (6)$$

subject to:

$$\|(x_m^{\text{BS}}, y_m^{\text{BS}}) - (x_n^{\text{NB}}, y_n^{\text{NB}})\|_2 \leq 200 \text{ m},$$

where $R_m^{\text{BS}} = 1/m \sum_{i=1}^{m} \log_2 \left(1 + RSS_i^{\text{BS}}/N_0\right)$, RSS_i^{BS} is the received signal strength at the ith TP on the DBIUP of the BS $r_n^{\text{NB}} = 1/n \sum_{j=1}^{n} \log_2 \left(1 + RSS_j^{\text{NB}}/N_0\right)$, RSS_j^{NB} is the received signal strength at the jth TP on DBIUP of the NB, N_0 is the noise power, $(x_{\text{BS}}, y_{\text{BS}})$ and $(x_{\text{NB}}, y_{\text{NB}})$ are the 2-D coordination of the BS and its NB, respectively, $(x_m^{\text{BS}}, y_m^{\text{BS}})$ and $(x_n^{\text{NB}}, y_n^{\text{NB}})$ are the 2-D coordination of the mth TP and nth TP on the DBIUPs of BS and its NB, respectively, and is $d_{mn} = \|(x_{\text{BS}}, y_{\text{BS}}) - (x_m^{\text{BS}}, y_m^{\text{BS}})\|_2 + \|(x_m^{\text{BS}}, y_m^{\text{BS}}) - (x_n^{\text{NB}}, y_n^{\text{NB}})\|_2 + \|(x_{\text{NB}}, y_{\text{NB}}) - (x_n^{\text{NB}}, y_n^{\text{NB}})\|_2$ the distance between BS and its NB going through two TPs where

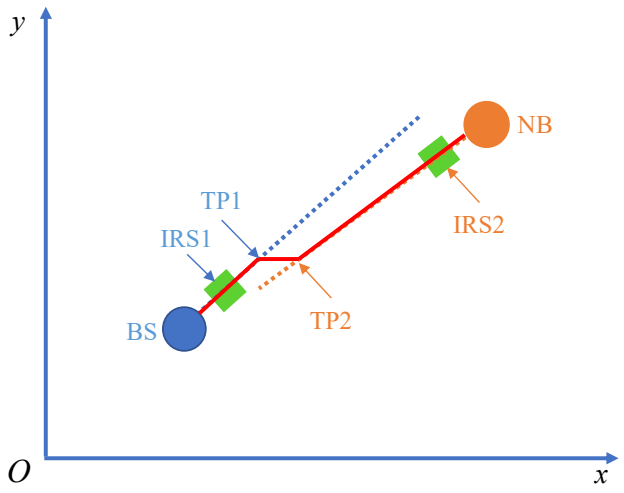

Fig. 3. The BIUP of a BS and its NB.

the $\|.\|_2$ is the ℓ_2-norm used to infer the distance of the vector coordinate from the origin.

The procedure of GA-based BIUP is depicted as follow:

Step 1 (Algorithm setup): Define the necessary system parameters for evaluating the fitness function in step 3: Set max_iter as the maximum number of iteration, the number

of population NP, the crossover probability p_c, the number of pair of chromosomes $K = p_c \times NP$, the crossover probability p_m, reset the iteration counter $iter\_count = 0$.

Step 2 (Population initiation): Randomly generate a population $P_{[0]} = \{Chr_1^{[0]}, Chr_2^{[0]}, \cdots, Chr_{2K}^{[0]}\}$ consisting of $2K$ chromosomes within their range (as mentioned in (6)).

Step 3 (Evaluation and selection): Calculate the fitness values of all chromosomes in $P_{[iter\_count]}$ then rank them based on their fitness values. We apply the roulette wheel selection (RWS) technique to accumulate good chromosomes. Let $\hat{P}_{[iter\_count]}$ denote the population after selection. The best chromosome $\mathrm{Chr}_{\text{best}}$ is saved for the next generation.

Step 4 (Reproduction): Define the off-springs by randomly select K chromosome pairs from $\hat{P}_{[iter\_count]}$ then perform the uniform crossover with the probability p_c using the whole arithmetic recombination technique [21], [22]. After that, the mutation is taken place with the probability p_m. Next, $\mathrm{Chr}_{\text{best}}$ is kept as one of chromosome of the current population. This step results in the next population $P_{iter\_count+1}$.

Step 5 (Loop/Termination): Increase the iteration counter (i.e., $iter\_count + 1$). Repeat step 3, 4 until $iter\_count$ reach max_iter and $\mathrm{Chr}_{\text{best}}$ is the optimal solution which contains the data rates at two TPs on their DBIUPs and the distance between 2 BSs passing though those TPs. The thoroughly connection of the BS, two TPs and NB is the optimal BIUP.

B. PSO-based BIUP Optimization

The PSO has been proven to be the robust and fast scholastic global optimization algorithm in solving non-linear, continuous variables and multimodal problem [22], [23]. As its indicated name. PSO consists of a swarm of particles, derived from real life as a group of flying birds. In our PSO, the position of each particle in search space represents for a potential solution to the optimization problem. We look for the good solution by moving the particles around the search space, then let them amend their moving by together exchange their information. For our optimization problem, the location of a particle is defined as a vector $p = [R_m^{\text{BS}}, R_n^{\text{NB}}, d_{mn}]$ which is similar to the Chr of the aforementioned GA optimization. This PSO optimization uses the similar fitness function to (6) which is given as:

$$f(p) = \left(\begin{array}{l} R_m^{\text{BS}} + R_n^{\text{NB}} \\ + \left(\begin{array}{l} \|(x_{\text{BS}}, y_{\text{BS}}) - (x_m^{\text{BS}}, y_m^{\text{BS}})\|_2 \\ +\|(x_m^{\text{BS}}, y_m^{\text{BS}}) - (x_n^{\text{NB}}, y_n^{\text{NB}})\|_2 \\ +\|(x_{\text{NB}}, y_{\text{NB}}) - (x_n^{\text{NB}}, y_n^{\text{NB}})\|_2 \end{array} \right)^{-1} \end{array} \right), \quad (7)$$

subject to:

$$\|(x_m^{\text{BS}}, y_m^{\text{BS}}) - (x_n^{\text{NB}}, y_n^{\text{NB}})\|_2 \leq 200 \text{ m},$$

The procedure of PSO-based BIUP is described as follows:

Step 1 (Algorithm setup): Define the necessary system parameters for evaluating the fitness function in step 3: Set max_iter as the maximum number of iteration, the number of particles NP, the inertia weight ω, the cognitive scaling factor c_{local}, social scaling factor c_{global} and the position boundary b_{min}, b_{max}; reset the iteration counter $iter\_count = 0$.

Step 2 (Population initiation): Randomly generate a population $P_{[iter\_count]} = \{p_{[iter\_count]}^{[1]}, p_{[iter\_count]}^{[2]}, \cdots, p_{[iter\_count]}^{[NP]}\}$ within their range (as mentioned in (7)). Then, initiate the local best position of each particle, $\mathbf{P}_{local}^{[\ell]}$ and the global best position of the population, $\mathbf{P}_{global}$ by inferring from the fitness function.

Step 3 (Evaluation and information exchange): Evaluate the fitness values for all particles $p_{[iter\_count]}^{[\ell]}, \ell = 1, \cdots, NP$ then only update the $\mathbf{P}_{local}^{[\ell]}$ and $\mathbf{P}_{global}$ when there are existing better positions.

Step 4 (Velocity and position update): Update the velocity of each particle using:

$$\begin{aligned} V_{[iter\_count+1]}^{[\ell]} =& \omega V_{[iter\_count]}^{[\ell]} \\ &+ c_{local} r_1 (\mathbf{P}_{local}^{[\ell]} - p_{[iter\_count]}^{[\ell]}) \\ &+ c_{global} r_2 (\mathbf{P}_{global} - p_{[iter\_count]}^{[\ell]}), \end{aligned} \quad (8)$$

where r_1 and r_2 are random number between 0 and 1; $V_{[iter\_count]}^{[\ell]}$ is the current velocity of $p_{[iter\_count]}^{[\ell])}$. The new position of each particle is amended as:

$$p_{[iter\_count+1]}^{[\ell]} = p_{[iter\_count]}^{[\ell]}) + V_{[iter\_count+1]}^{[\ell]} \quad (9)$$

The nearest vertex approach (NVA) [23] is applied to approximate the valid position defined as $\hat{p}_{[iter\_count+1]}^{[\ell]}$ since the index of $p_{[iter\_count+1]}^{[\ell]}$ may not integers after applying (9). The position of a particle is then validated whether it is out of the boundary or not. We adopt the reflecting bound-handling scheme [24] to deal with the out-of-bound particles. The new population is:

$$\hat{P}_{[iter\_count]} = \{\hat{p}_{[iter\_count]}^{[1]}, \hat{p}_{[iter\_count]}^{[2]}, \cdots, \hat{p}_{[iter\_count]}^{[NP]}\} \quad (10)$$

Step 5 (Loop/Termination): Increase the iteration counter (i.e., $iter\_count + 1$). Repeat step 3, 4 until the $iter\_count$ reach the max_iter and the final $\mathbf{P}_{global}$ is the optimal solution consisting the information of the data rate at two TPs on their DBIUPs and the distance between 2 BSs passing though those TPs. The thoroughly connection of the BS, two TPs and the NB is the optimal BIUP.

IV. Simulation Results and Discussion

In Section II-B, we have demonstrated the results of the DBIUP map as the preliminary inferred theoretical results of our IRS scheme. In this section, the efficiency of the optimization algorithms on our problem in improving the CADR and the DD of the DBIUP map is presented.

In Fig. 4, the CADR versus various three key factors, namely the number of IRS panels, the BS Tx power and the IRS sizes are illustrated. The total of data rate over the entire area is depicted in Fig. 4(a). With 30 W of the Tx power, the sum of data rate is proportional to the RT sizes and the number of IRSs deployed over the region. Specifically, the sum of data rate with 6 IRSs/BS is twice to three times higher than that of the deployment of 4 IRSs/BS. The reason is that the more IRSs panels surrounding the BS, the more possible DBIUPs

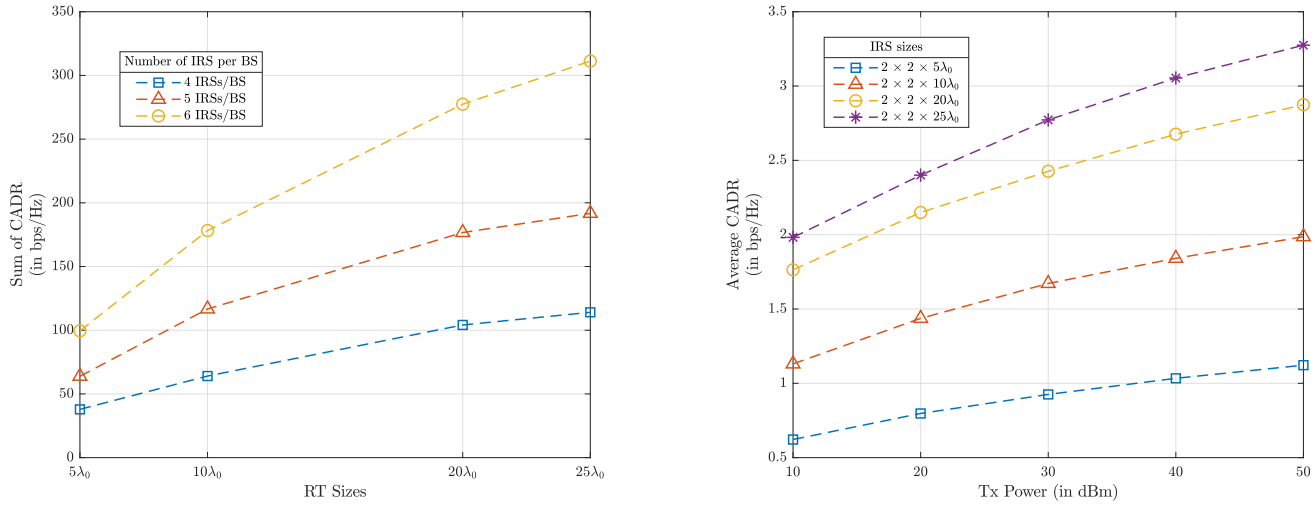

(a) (b)

Fig. 4. (a) The total CADR over the map and (b) the average CADR of a BIUP.

the map contains which lead to the significant increment in the total data rate. On the other hand, this figure also reveals the effective contribution of the RT sizes in the rise of the data rate over the map. Specifically, there is a notably jump from approximated 100 bps/Hz at RT size of $5\lambda_0$ to more than 310 bps/Hz with RT size of $25\lambda_0$ for the case of 6 IRSs/BS. Furthermore, we take into consideration the effectiveness of the Tx power of BS and show it in Fig. 4(b) with 6 IRSs per each BS. Generally, there is a gradually surge of the average CADR over all BIUPs for each IRS size when the Tx power raises which meets our expectation. The average CADR of a BIUP with IRS size of $2 \times 2 \times 5\lambda_0$ grows by 0.1 bps/Hz from around 0.6 bps/Hz to a little higher than 1.1 bps/Hz when then Tx power increases by 10 W from 10 to 50 W while the increase step of the average CADR of IRS size $2 \times 20 \times 25\lambda_0$ is notably higher at around 0.4 bps/Hz.

The DD of the UAV when travelling among BSs over the map is demonstrated in Fig. 5. Generally speaking, the number of deployed IRSs take more efficiency than the RT size and the Tx power into the total DD of the IRS network scheme. More specifically, the Fig. 5(a) illustrates the sum of DD over the various RT sizes and number of IRSs when the Tx power is 30 W. The noteworthy reduction of DD can be witnessed as the increase of number of IRSs with the decrease from more than 25 km of DD of 4 IRSs/BS to lower 10 km of 6 IRSs/BS while the difference of DDs over all RT sizes with the same number of equipped IRS are not too significant. In addition, in the Fig. 5(b), when the Tx power is equal or higher than 30 W and the quantity of IRSs/BS is six, the sum of DD becomes stable even the differences in the IRS sizes. Furthermore, there is an interesting thing to note is that the bigger the IRS size is, the less influence of the Tx power contributes. The notable drop can be revealed when the Tx power increase from 10 to 20 W, the DD is considerably fallen from around 15 km to just over 10.5 km with the RT size of $2 \times 2 \times 5\lambda_0$.

Next, we consider the efficiency of two HA-based BIUP algorithms which are employed for our optimization problem. The optimal system parameters of both algorithms are illustrated in the Table III after several trials to get the best solutions by evaluating the fitness values of the objective function (7). In Fig. 6(a), we achieve the sum of data rate over different number of installed IRSs by adopting GA and PSO algorithms which are closed to that of the exhaustive search. It can prove that those two HAs are suitable for our optimization problem. In general, the GA outperforms the PSO algorithm in the effectiveness and the convergence for dealing with our optimization problem. The reason is that the PSO has to approximate the indexes of the particle to get the valid positions by using the NVA method. Because of this reason, the aforementioned figures of CADR and DD are prepared using best results obtained from GA. More specifically, the Fig. 6(b) shows the comparison between GA and PSO in the average CADR when deploying 6 IRSs/BS, 10 to 50 W of Tx power and the RT sizes from $5\lambda_0$ to $25\lambda_0$. For each pair of number of IRSs and Tx power, the GA always show its better performance as the higher CADR. The same phenomenon can be also witnessed when considering the impact of RT size and number of IRSs to the CADR as show in Fig. 6(c). In addition, the IRS networks with different number of IRSs/BS and IRS sizes are also constructed for attaining the number of total disconnections over the map. The Fig. 6(d) illustrates that the total gap during UAV flying path when solving the optimization problem using GA is less than that of the results obtained from PSO algorithm at all cases of RT sizes and the quantity of IRS.

Additionally, we verify the convergence of two HA-based BIUP algorithms over 100 iterations which is shown in Fig. 7 with $10\lambda_0$ and $25\lambda_0$ of the RT sizes, 10 and 50 W of the Tx power. At the first iteration, both algorithms received very high fitness values but the GA quickly converged as it reaches to the optimum values after 15–20 iterations while the PSO takes around 80–90 iterations to obtain the optimal solution.

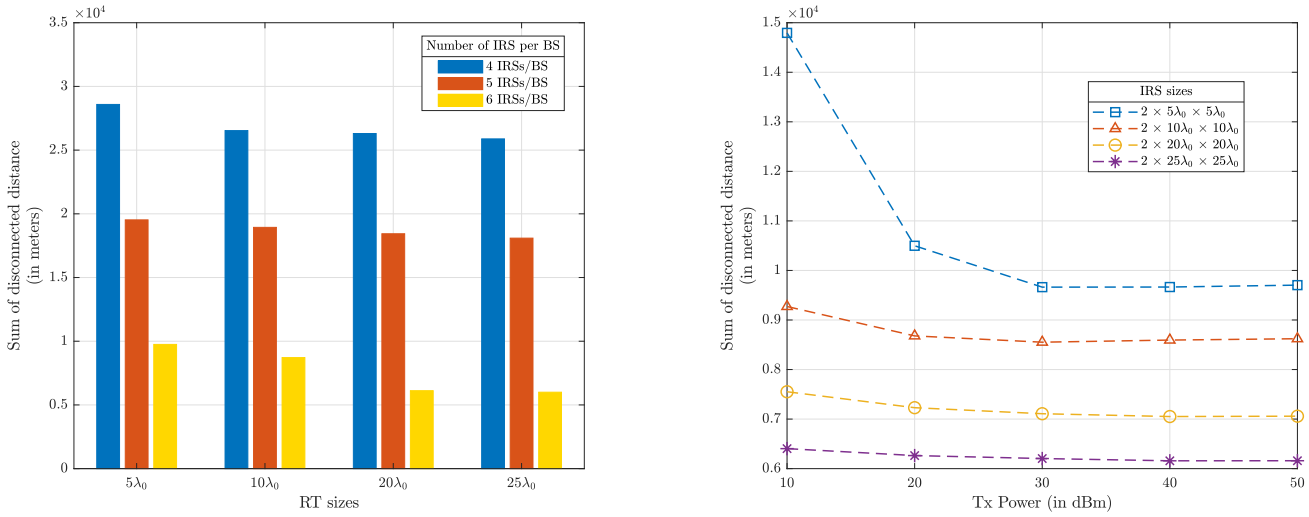

(a) (b)

Fig. 5. The total disconnected distance over the map with (a) various IRSs/BS and (b) various IRS sizes.

TABLE III
THE SYSTEM PARAMETERS OF GA AND PSO ALGORITHMS.

GA		PSO	
NP	150	NP	150
p_c	0.99	ω	0.7298
p_m	0.5	c_{local}	1.4962
max_iter	100	c_{global}	1.4962
$iter\_count$	0	max_iter	100
		$iter\_count$	0

Moreover, the converged fitness values of the GA also present superior solution than PSO at the end of 100 iterations.

V. CONCLUSIONS

In this paper, we investigated and optimized the achievable data rate and disconnected distance of an IRS-assisted uplink communication scheme to support the UAV in urban area without any change to the exiting terrestrial infrastructure. The RSS model of the IRS network containing the far-field path loss was constructed by adopting the physical optics techniques. We constructed the DBIUP map utilizing the RSS model and the optimal configuration of the IRS network. Two HAs, namely the GA and PSO were employed to optimized the CADR, the UAV operational direction and possible BIUPs. The numerical results showed that the DBIUP map gave its essential contribution to our optimization problem while the GA performed the superior ability in effectiveness and convergence. Additionally, the efficiencies of three key factors, i.e., Tx power, the IRS size and the quantity of deployed IRSs were taken into consideration. The trends of optimal CADR and DD are revealed. In detail, the sum of CADR over the region is significantly enhanced when adding more IRSs surrounding each BS. On the other hand, the IRS size also plays an important role in enhancing the CADR; moreover, the larger size the IRS yields the greater CADR. On contrary, the DD followed an opposite trend of the CADR. More specifically, the DD was inversely proportional to the increment of the Tx power, the number of IRS and IRS size. The Tx power took less influence to the DD when the IRS size is large while the number of IRS and the IRS size are the main components affecting to the DD of the map.

APPENDIX A
PROOF OF THE CALCULATIONS IN PROPOSITION 1

Note that the $O_{r,\theta,\phi}$ spherical coordinate system sharing the same origin with the $O_{x,y,z}$ coordinate system in our investigation. Let analyze the electric current density on the surface of the IRS ($z = 0$). By neglecting surface edge effects and applying the physic optic technique on the negligible-thickness flat IRS [20, Ch. 7.10], the electric current density can be expressed as:

$$\mathbf{J}_s \approx 2\mathbf{e}_z \times \mathbf{H}_{\text{inc}} = -2\mathbf{e}_x \frac{E_{\text{ref}} \cos(\theta_{\text{ref}})}{\eta} e^{-j\beta \sin\theta_{\text{ref}} y + j\phi_0} \quad \text{(A1)}$$

Using Descartes-to-spherical coordination transformation and following the similar steps as in [20, Example 6-4], vector potential can is calculated as:

$$\begin{aligned}\mathbf{A} &= \frac{\mu e^{-jkd}}{4\pi d} \\ &\quad \times \iint_S \left(J_s \sin\theta\cos\phi \cdot \vec{\mathbf{i}_r} + J_s \cos\theta\cos\phi \cdot \vec{\mathbf{i}_\theta} - J_s \sin\phi \cdot \vec{\mathbf{i}_\phi} \right) \\ &\quad \times e^{jkr\cos\psi} dx' dy' \\ &= \frac{\mu e^{-jkd}}{4\pi d} (\mathbf{N}_r + \mathbf{N}_\theta + \mathbf{N}_\phi), \end{aligned} \quad \text{(A2)}$$

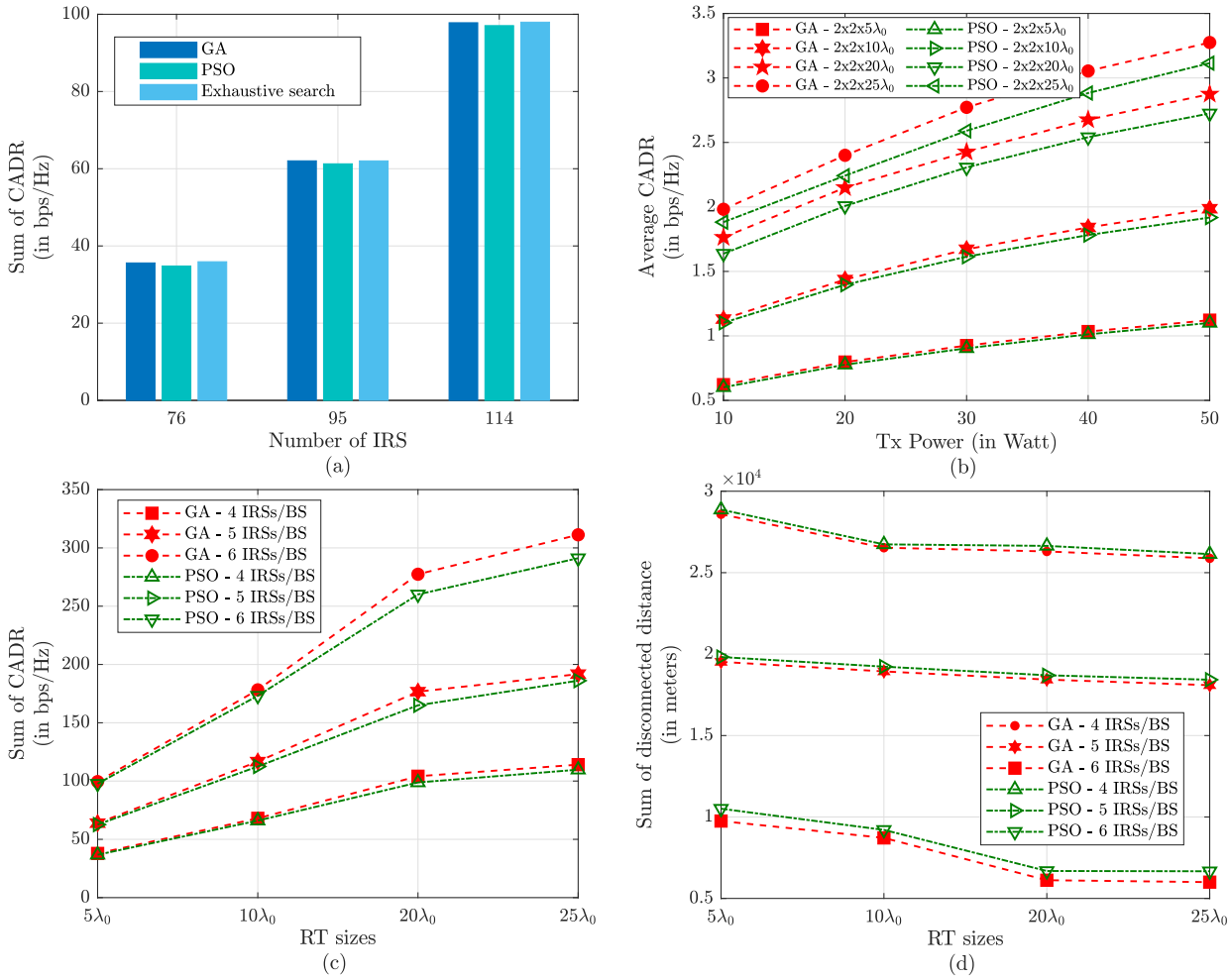

Fig. 6. The effectiveness of the GA and PSO algorithms on: (a) Sum of CADR over number of IRS, (b) average CADR over Tx power and IRS sizes, (c) Sum of CADR and (d) Total DD over RT sizes and number of IRS.

where

$$\mathbf{N}_\theta = -2\frac{E_{\text{ref}}}{\eta}\cos\theta_s\cos\phi_s\cos(\theta_{\text{ref}}) \times \int_{-\frac{a}{2}}^{\frac{a}{2}} e^{jkx'\sin\theta_s\cos\phi_s}\,dx' \times \int_{-\frac{b}{2}}^{\frac{b}{2}} e^{jky'\sin\theta_{\text{ref}}-\sin\phi_s\sin\phi_s}\,dy', \tag{A3}$$

$$\mathbf{N}_\phi = -2\frac{E_{\text{ref}}}{\eta}\sin\phi\cos(\hat{\theta}_r)e^{j\phi} \times \int_{-\frac{a}{2}}^{\frac{a}{2}} e^{jkx'\sin\theta\cos\phi}\,dx' \times \int_{-\frac{b}{2}}^{\frac{b}{2}} e^{jky'(\sin\theta\sin\phi-\sin(\hat{\theta}_r))}\,dy', \tag{A4}$$

$$\mathbf{N}_r = 0 \tag{A5}$$

Using the fact that $\int_{-\frac{c}{2}}^{\frac{c}{2}} e^{jaz}\,dz = c[\frac{\sin(a\frac{c}{2})}{a\frac{c}{2}}]$ [20, Example 6-4], (A3) and (A4) can be written as

$$\mathbf{N}_\theta = -2\frac{abE_{\text{ref}}\cos(\theta_{\text{ref}})}{\eta}\cos\theta_s\cos\phi_s \times \frac{\sin(\frac{1}{2}ak\sin\theta_s\cos\phi_s)}{\frac{1}{2}ak\sin\theta_s\cos\phi_s} \times \frac{\sin(\frac{1}{2}bk(\sin(\theta_{\text{ref}})-\sin\theta_s\sin\phi_s))}{\frac{1}{2}bk(\sin(\theta_{\text{ref}})-\sin\theta_s\sin\phi_s)} \tag{A6}$$

$$\mathbf{N}_\phi = -2\frac{abE_r\sin\phi\cos(\hat{\theta}_r)e^{j\phi}}{\eta} \times \frac{\sin(\frac{1}{2}ak\sin\theta\cos\phi)}{\frac{1}{2}ak\sin\theta\cos\phi} \times \frac{\sin(\frac{1}{2}bk(\sin\theta\sin\phi-\sin(\hat{\theta}_r)))}{\frac{1}{2}bk(\sin\theta\sin\phi-\sin(\hat{\theta}_r))} \tag{A7}$$

Using approximation $\mathbf{E}_{\{\theta,\phi\}} \simeq -j\omega\mathbf{A}_{\{\theta,\phi\}}$ [20, eq. (6-117)], $S(\theta_s,\phi_s) = |\mathbf{E}_{\theta_s}|^2 + |\mathbf{E}_{\phi_s}|^2$, and $4\pi d\eta(\omega\mu)^{-1} = 2\lambda d$, the

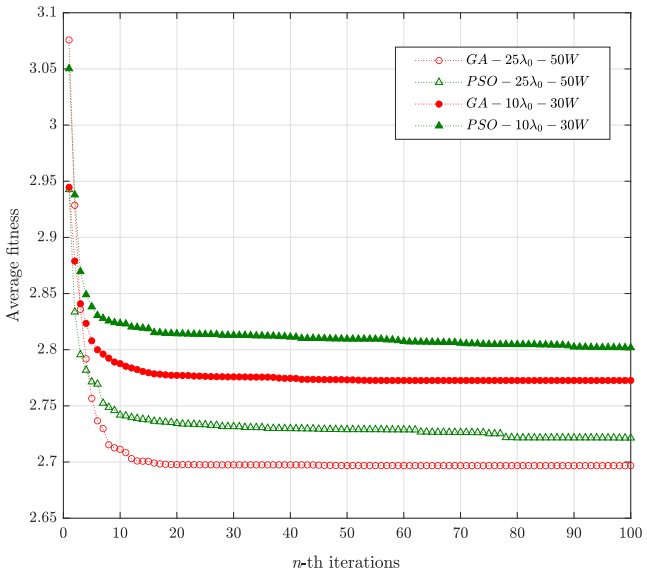

Fig. 7. The convergence of HA-based BIUP algorithms.

squared magnitude of the scattered field is calculated as

$$S(\theta_s,\phi_s)=\left(\frac{\omega\mu}{4\pi d}\right)^2\left(|\mathbf{N}_{\theta_s}|^2+|\mathbf{N}_{\phi_s}|^2\right) \tag{A8}$$

Substituting (A6) and (A7) into (A8), Proposition 1 can be proven.

REFERENCES

[1] M. Mozaffari *et al.*, "A tutorial on UAVs for wireless networks: Applications, challenges, and open problems," *IEEE Commun. Surveys Tuts.*, vol. 21, no. 3, pp. 2334–2360.

[2] K. P. Valavanis and G. J. Vachtsevanos, *Handbook of Unmanned Aerial Vehicles*, Amsterdam, The Netherlands: Springer, 2014.

[3] Y. Zeng, R. Zhang, and T. J. Lim, "Wireless communications with unmanned aerial vehicles: Opportunities and challenges," *IEEE Commun. Mag.*, vol. 54, no. 5, pp. 36–42, May 2016.

[4] S. Konatowski and P. Pawłowski, "Ant colony optimization algorithm for UAV path planning," in *Proc. IEEE TCSET*, Feb. 2018, pp. 177–182.

[5] H. Xu, S. Jiang and A. Zhang, "Path planning for unmanned aerial vehicle using a mix-strategy-based gravitational search algorithm," *IEEE Access*, vol. 9, pp. 57033–57045, 2021.

[6] A. Al-Hourani, S. Kandeepan and A. Jamalipour, "Modeling air-to-ground path loss for low altitude platforms in urban environments," in *Proc. IEEE GLOBECOM*, Dec. 2014, pp. 2898–2904.

[7] S. Alfattani *et al.*, "Aerial platforms with reconfigurable smart surfaces for 5G and beyond," *IEEE Commun. Mag.*, vol. 59, no. 1, pp. 96–102, Jan. 2021.

[8] X. Pang *et al.*, "When UAV meets IRS: Expanding air-ground networks via passive reflection," *IEEE Wireless Commun.*, vol. 28, no. 5, pp. 164–170, Oct. 2021.

[9] Y. Wei *et al.*, "Channel estimation for IRS-aided multiuser communications with reduced error propagation," *IEEE Trans. Wireless Commun.*, vol. 21, no. 4, pp. 2725–2741, Apr. 2022.

[10] E. Basar *et al.*, "Wireless communications through reconfigurable intelligent surfaces," *IEEE Access*, vol. 7, pp. 116753–116773, Aug. 2019.

[11] Ö. Özdogan, E. Björnson, and E. G. Larsson, "Intelligent reflecting surfaces: Physics, propagation, and pathloss modeling," *IEEE Wireless Commun. Lett.*, vol. 9, no. 5, pp. 581–585, May 2020.

[12] D. Zhang *et al.*, "Mobile user trajectory tracking for IRS enabled wireless networks," *IEEE Trans. Veh. Technol.*, vol. 70, no. 8, pp. 8331–8336, Aug. 2021.

[13] Q. Wu and R. Zhang, "Towards smart and reconfigurable environment: Intelligent reflecting surface aided wireless network," *IEEE Commun. Mag.*, vol. 58, no. 1, pp. 106–112, Jan. 2020.

[14] C. Huang *et al.*, "Holographic MIMO surfaces for 6G wireless networks: Opportunities, challenges, and trends," *IEEE Wireless Commun.*, vol. 27, no. 5, pp. 118–125, Oct. 2020.

[15] Z. Wei *et al.*, "Sum-rate maximization for IRS-assisted UAV OFDMA communication systems," *IEEE Trans. Wireless Commun.*, vol. 20, no. 4, pp. 2530–2550, Apr. 2021.

[16] S. Fang, G. Chen, and Y. Li, "Joint optimization for secure intelligent reflecting surface assisted UAV networks," *IEEE Wireless Commun. Lett.*, vol. 10, no. 2, pp. 276–280, Feb. 2021.

[17] M. Hua *et al.*, "UAV-assisted intelligent reflecting surface symbiotic radio system," *IEEE Trans. Wireless Commun.*, vol. 20, no. 9, pp. 5769–5785, Sep. 2021.

[18] S. Jiao *et al.*, "Joint beamforming and phase shift design in downlink UAV networks with IRS-sssisted NOMA," *J. Commun. Inf. Networks*, vol. 5, no. 2, pp. 138–149, Jun. 2020.

[19] Z. Mohamed and S. Aïssa, "Leveraging UAVs with intelligent reflecting surfaces for energy-efficient communications with cell-edge users," in *Proc. ICC*, Jun. 2020, pp. 1–6.

[20] C. A. Balanis, *Advanced Engineering Electromagnetics*, 2nd ed. Hoboken, NJ, USA: Wiley, 2012.

[21] J. Kennedy and R. Eberhart, "Particle swarm optimization," in *Proc. IEEE ICNN*, Nov.–Dec. 1995, pp. 1942–1948.

[22] Y. Shi and R. Eberhart, "A modified particle swarm optimizer," in *Proc. IEEE ICEC*, May. 1998, pp. 69–73.

[23] S. Chowdhury, W. Tong, and A. Messac. "A mixed-discrete particle swarm optimization algorithm with explicit diversity-preservation," *Structural Multidisciplinary Optim.*, vol. 47, pp. 367–388, 2013.

[24] T. Huang and A. S. Mohan, "A hybrid boundary condition for robust particle swarm optimization," *IEEE Antennas Wireless Propag. Lett.*, vol. 4, pp. 112–117, Jun. 2005.

Pham The Hien received the B.E. degree in Communication and Networking from HoChiMinh City University of Transport, Vietnam, in 2012. He is currently pursuing an M.S. in Information and Communication Engineering, Kongju National University, Korea. His major research interests are nondestructive testing, structure health monitoring, communication and networking, wireless communication systems, and optimization methods.

Van Phu Tuan received the B.E. and M.E. degrees in Electronics and Telecommunications Engineering from the Ho Chi Minh City University of Technology (HCMUT), Vietnam, in 2010 and 2013, respectively, and the Ph.D. degree in Electrical Engineering from the University of Ulsan (UOU), Ulsan, South Korea, in 2018. From 2018 to 2019 and from 2019 to 2021, he was respectively a Postdoctoral Researcher with the UOU and Kongju National University (KNU), Cheonan, South Korea. He is currently working with Dong A university (UDA), Da Nang, Vietnam. His major research interests include wireless communications systems, physical layer security, wireless powered communications, IRS-aided wireless communication, machine learning and optimization methods.

Ic Pyo Hong (Member, IEEE) received the B.S., M.S., and Ph.D. degrees in Electronics Engineering from Yonsei University, Seoul, South Korea, in 1994, 1996, and 2000, respectively. From 2000 to 2003, he was with the Information and Communication Division, Samsung Electronics Company, Suwon, South Korea, where he was a Senior Engineer with CDMA Mobile Research. He was a Visiting Scholar with Texas A&M University, College Station, TX, USA, in 2006, and Syracuse University, Syracuse, NY, USA, in 2012. Since 2003, he has been with the Department of Information and Communication Engineering, Kongju National University, Cheonan, South Korea, where he is currently a Professor. His research interests include numerical techniques in electromagnetics, periodic electromagnetic structures and its applications in wireless communications.